Interfacial Behavior of Polymer Electrolytes.

John B. Kerr*, Yong Bong Han, Gao Liu, Craig Reeder, Jiangbing Xie and Xiaoguang Sun.

Lawrence Berkeley National Laboratory,
MS 62R0203, 1 Cyclotron Road,
Berkeley, California, 94602, USA
jbkerr@lbl.gov

Abstract.

Evidence is presented concerning the effect of surfaces on the segmental motion of PEO-based polymer electrolytes in lithium batteries. For dry systems with no moisture the effect of surfaces of nano-particle fillers is to inhibit the segmental motion and to reduce the lithium ion transport. These effects also occur at the surfaces in composite electrodes that contain considerable quantities of carbon black nano-particles for electronic connection. The problem of reduced polymer mobility is compounded by the generation of salt concentration gradients within the composite electrode. Highly concentrated polymer electrolytes have reduced transport properties due to the increased ionic cross-linking. Combined with the interfacial interactions this leads to the generation of low mobility electrolyte layers within the electrode and to loss of capacity and power capability. It is shown that even with planar lithium metal electrodes the concentration gradients can significantly impact the interfacial impedance. The interfacial impedance of lithium/PEO-LiTFSI cells varies depending upon the time elapsed since current was turned off after polarization. The behavior is consistent with relaxation of the salt concentration gradients and indicates that a portion of the interfacial impedance usually attributed to the SEI layer is due to concentrated salt solutions next to the electrode surfaces that are very resistive. These resistive layers may undergo actual phase changes in a non-uniform manner and the possible role of the reduced mobility polymer layers in dendrite initiation and growth is also explored. It is concluded that PEO and ethylene oxide-based polymers are less than ideal with respect to this interfacial behavior.

Introduction.

The mechanisms of ion transport in dry and gel polymer electrolytes and polyelectrolytes has been the subject of much interest due to their use as separators in rechargeable lithium batteries and fuel cells. While the simplest approach is to investigate the motion through the bulk of the membrane, much of the critical ion transport occurs close to the electrode surfaces which are frequently high surface area composites with complex morphologies. Since its known that the mobility of polymers is considerably altered in the presence of nanoparticles[1,2] and surfaces[3], it is important to investigate the ion motion in the regions close to the electrodes. Battery system modeling of gel and dry polymer systems[4-7] shows that much of the performance loss occurs in the composite structures where the ion transport properties can be quite different from the bulk due to the influence of the surfaces. The recent intense interest in the use of ceramic nanoparticle filler material to alter the transport properties of lithium salts in polymer electrolytes[8-19] has generated a considerable body of useful data in this respect that can be used to understand the behavior of composite electrodes as well as membranes.

The transport of lithium ions to the surface of lithium metal electrodes is one of a number of critical factors in the growth of dendrites, which can lead to coulombic inefficiency, side reactions, short circuiting of the cell and the formation of mossy lithium, a serious safety issue. Dendrites certainly grow if the current density exceeds the limiting current density[20-22], which is determined by the salt concentration, the cell geometry and the transport properties of the electrolyte. In the case of a binary salt polymer electrolyte, the transport properties are the conductivity (σ), the salt diffusion coefficient(D_s) and the transference number (t_+^o). The transport properties are generally

measured as bulk properties and therefore any changes in these properties that occur as a result of the presence of the electrode interfaces can induce the growth of dendrites at unexpectedly low current densities. It has long been observed that dendrite growth also occurs at current densities well below the limiting current[23,24] and the factors that influence the initiation[25,26] and propagation[27-29] of dendrite growth are a multifaceted problem that includes transport properties, interfacial properties and mechanical properties of the electrolytes in addition to the properties and possible non-uniformity of the Solid Electrolyte Interphase (SEI)[30] on the lithium metal. Hence the understanding of the behavior of polymer electrolytes at interfaces is of considerable importance to the efficiency and safe operation of lithium metal batteries and some initial observations are presented in this paper

Experimental

PPO (Parel) was a gift from Zeon chemical and was purified by soxhlet extraction with methanol and then dried under vacuum over P_2O_5 in a drying pistol prior to introduction to the glove-box. PEO samples were obtained form Dow Chemical. PEO (Polyox WSR-301, Mw = 5×10^6 and Polyox WSR-N80, Mw = 2×10^5) was recrystallized from acetone to remove butylhydroxytoluene (BHT) stabilizer, and was defined as lab-purified PEO. From the product Material Safety Data Sheet, these polymers contain up to 4 wt.% fumed silica and calcium salt residues. The recrystallization process does not remove these additives. Polyox WSR-N80 with all additives removed is defined as ultra-pure PEO and was prepared according to a method that is described in detail elsewhere[31]. All PEO samples were dried under vacuum at 50^{o}C over P_2O_5 overnight before storing in the dry box. LiTFSI (Li $N(SO_2CF_3)_2$) a gift from 3M, LiTf ($LiCF_3SO_3$)

(Aldrich) and $LiClO_4$ (Alfa Aesar) were dried under vacuum over P_2O_5 in a drying pistol at 160^oC and transferred to dry box without exposure to air. V_6O_{13} (KM VANOX-13) was a gift from Kerr-McGee Corporation and prepared as composite electrodes with PEO-LiTFSI and acetylene black(Chevron) using a solvent slurry coating on stainless steel. Polytrimethylene oxide (PTMO) was prepared by cationic ring-opening polymerization of oxetane with BF_3-etherate. The PTMO was fractionated three times using THF and Hexane mixture solvent and dried under high vacuum. GPC analysis of of the pure PTMO polymer using THF eluent and a PLGel Mixed B column gave Mw = 65,000. PDI = 5.7.

Fumed silica from Degussa with a hydrophilic surface (Aerosil 200, 12nm id particle size) and a hydrophobic surface (Aerosil R805, 12nm id particle size) and alumina (neutral, 5.8nm id particles size) from Aldrich were dried under 160^oC vacuum over P_2O_5 for 2 days before stored in dry box. Acetonitrile and glyme were obtained from Burdick & Jackson with highest purity (>99.9%) and lowest water content (<0.001%) available. Prior to use, they were dried in the "solvent" glove box by percolation through a column of Super-activated Alumina (ICN).

Two glove boxes were used in the experiments. One is defined as the "solvent" glove box which was used for solvent-involved operations such as dissolving, film casting, etc. The other is defined as the "dry" glove box which was scrupulously free of organic solvent vapors. It was used for the storage of dry chemicals and samples, cell assembly, etc. Both glove boxes were filled with helium with H_2O and O_2 concentrations <1ppm. Unless otherwise mentioned, the dry box stands for "dry" glove box.

The polymers, salts, and fillers (measured in weight percent of lab-purified PEO) were weighed in the dry box and transferred in capped bottles to the "solvent" glove box. They were dissolved in dried acetonitrile and the solutions were cast on Teflon plates. The solvent was evaporated and the resulting films were fully dried in the vacuum anti-chamber of the "solvent" glove box at room temperature. The films were then transferred in sealed containers to the "dry" glove box. The films were assembled in Swagelok cells in the dry box with two stainless-steel electrodes. A spacer ring with known thickness and central area was used to control the dimensions of polymer electrolytes between the two blocking electrodes. The Swagelok cell is designed to exert controlled pressure on the cell sandwich and completely sealed to allow measurement outside of the dry box. The cells were taken out of the dry box and cured at ~110^{o}C overnight in a convection oven with temperature control within ±0.5^{o}C. Under high temperature and pressure, the polymers melt, flow and completely fill the central hole of the spacer. To assess the effect of exposure to atmosphere, the cells were opened and the sample allowed to rest in ambient air for up to 72 hours. The cells were then reassembled and resealed for measurements. Control cells were opened in the dry box and then resealed for comparison.

A Solartron SI 1254 four-channel frequency response (65 kHz to 0.01Hz) analyzer and a 1286 electrochemical interface were used to measure the AC conductivity. The measurements were carried out in cooling scan unless otherwise mentioned. The cells were equilibrated in the oven for at least one hour before the conductivity was measured. Measurements below room temperature were taken by placing cells in a laboratory refrigerator. The dynamic mechanical thermal analysis (DMTA) was

conducted on a Rheometric RSAII Solids Analyzer in compression mode with a parallel plate apparatus. A refrigerant air drier was used to supply dry air; alternatively, nitrogen evaporated from a liquid N_2 dewar was used as the measurement atmosphere. However, it was not possible to prepare the samples for DMTA without exposure to atmosphere. To compensate for this the samples were heated at 110^{o}C for 30 minutes prior to drive off any absorbed moisture before quenching to the measurement temperature. Thermal measurements were performed on a Perkin-Elmer DSC-7 apparatus equipped with a nitrogen glove box. The furnace was purged with helium in measurement. The samples were sealed hermetically in aluminum sample containers in the dry box and then transferred to DSC glove box. A hole was punctured on the sample container to expose samples to purging gas and remove vapors in heating for certain non-dried samples.

Results and Discussion

Figure 1 shows two schemes that represent possible effects of surfaces on polymer dynamics. The first (1a) postulates that the interaction of the polymer with the solid surface leads to an immobile layer of polymer next to the surface plus a layer of polymer that is restricted in its motion in addition to polymer that is sufficiently far from the surfaces that it is unaffected by the presence of the filler. When the particles are sufficiently small and the concentration of particles are optimum, a second t_g may be observed in dynamic mechanical thermal analysis (DMTA) at temperatures up to 100^{o}C higher than the bulk t_g [32,1]. The presence of the two different relaxations in the presence of nano-particles has been confirmed by neutron scattering[33]. The second scheme (1b) , which is applicable to high Mw polymers, shows the interaction of the long

polymer chains with many particles and leads to restriction of the polymer motion with an increase in t_g [2]. In either case the effect is dependent upon the strength of the polymer-surface interaction. Figure 2 shows the effect on the glass transition of addition of fumed silica (Degussa A200, hydrophilic) to polypropylene oxide, as measured by DMTA. The tan δ curve is the ratio of the storage modulus (E' in this case) divided by the loss modulus (E") and is sensitive to changes in the polymer state such as the glass transition[34-36]. The height and area of the peak in the tan δ curve is an indication of the proportion of the polymer that is undergoing the transition[1] and progressively diminishes as proportion of filler nanoparticles is increased (% by weight in legend in Figure 2), demonstrating the complete immobilization of a portion of the polymer due to the presence of particle surfaces. The storage and loss moduli (not shown) of the polymer increase at temperatures above the t_g upon addition of fumed silica indicating the improvement in mechanical properties that is consistent with a decrease in the polymer motion. This decrease in motion is due to strong interactions between the polymer chains and the particle surfaces. Weston and Steele[37] reported on the improvements in mechanical strength of PEO electrolytes upon addition of the filler. They also noted that the conductivity of the filled polymer electrolytes decreased upon addition of filler, a result that is consistent with the immobilization of polymer motion if the mechanism of ion conduction is primarily linked to the segmental motion of the polymer[38,39]. Weston and Steele also noted that the behavior of PEO electrolytes was very dependent upon the preparation conditions[40] and recent results obtained in this laboratory[31] have demonstrated the critical importance of the presence of water and other impurities in the determination of transport properties.

It has been shown in this laboratory that the addition of nano-particulate ceramic fillers such as fumed silica or alumina to polymer electrolytes such as PEO-LiX (X = Triflate($CF_3SO_3^-$), Perchlorate(ClO_4^-) and bis(Trifluoromethylsulfonyl)imide (TFSI, $(CF_3SO_2)_2N^-$)), PPO-LiTFSI and PEMO-LiTFSI leads to an increase in the glass transition temperature, increases in the mechanical moduli in the rubbery state, decreased conductivity and decreased salt diffusion coefficients[31]. These observations were made under conditions where considerable care was taken to exclude moisture. For example, addition of hydrophilic fumed silica (A200) to PEO-$LiClO_4$ leads to a 20^0C increase in t_g and a large decrease in the glass transition tan δ peak size as well as an order of magnitude decrease in the conductivity. Similar observations are made with dry PEO-LiTFSI and PEO-LTf. This clearly demonstrates the relationship between the polymer segmental motion and the lithium ion transport properties in dry electrolytes. Modification of the surface of the filler material by covalent binding of hydrophobic octyl groups as in the case of R805 fumed silica modifies the effect of the surface-polymer interaction and leads to less inhibition of both ion transport and segmental motion. The presence of moisture and other impurities also alters the surface of filler additives such as silica or carbon black and leads to a change in the strength of the polymer-surface interaction that controls the polymer mobility next to the surface. Since the strength of the polymer-surface interaction has been shown to play a major role in the alteration of polymer dynamics[1], control over the surface is an important parameter. Since electrode interfaces also involve polymer chains next to surfaces, it is likely that similar effects will also control the polymer motion at the surfaces of electrodes such as carbon, metal oxides and lithium metal.

Figure 3 shows a schematic of a typical lithium metal-polymer battery with a composite cathode comprised of particles of an intercalation compound (30-50%), carbon black(10%) added to make electronic connection and the polymer electrolyte which binds the particles together and provides the ionic connection to the cathode surfaces. It is obvious that a large proportion of the polymer electrolyte chains are in close proximity to the surfaces of the cathode particles and the carbon black. Although the cathode particles are typically 1-10 μm in diameter the carbon particles are usually 20-100 nm in size and present a very large surface area for the polymer to interact with. The proportion of filler particles in the polymer is equivalent to between 20 and 50% which is similar to the amounts added to the PPO shown in Figure 2. If the lithium ion transport properties are dependent upon segmental motion of the polymer chains then it is reasonable to suppose that the transport properties within the composite electrode will be somewhat different from the those measured in the bulk membrane separator due to the confinement effect of the surfaces on polymer chain motion.

The bulk transport properties of PEO and PPO electrolytes with LiTFSI and LiTf have been reported[41-43] and generally the conductivities and salt diffusion coefficients decrease as the salt concentration increases above oxygen-lithium ratios of about 8:1. This behavior can be understood in view of the dependence of the glass transition temperature (t_g) on the concentration of salt. Examples are shown in Figure 4 for the amorphous polymers, PEMO (oxymethylene-linked PEG400), PPO and PTMO (poly(trimethylene oxide). The t_g is inversely related to the segmental motion of the polymer which decreases as the t_g increases. As can be seen from the figure, the t_g for the PPO and PEMO polymers increases rapidly as the salt concentration increases above 10:1

oxygen:Li ratio. The decrease in polymer mobility with salt concentration is attributed to ionic cross-linking due to the binding of the lithium ions to the polymer chains. The decrease in mobility apparently outweighs the increase in charge carrier concentration for these polymers resulting in a decrease in transport properties. The combination of high salt concentrations with surfaces that also inhibit polymer motion and further increase the t_g implies that close to surfaces the physical state of the polymer electrolyte may change to a much less mobile and even a glassy form and the ion transport properties will be quite different from those measured in the bulk of the separator. Thus the transport properties adjacent to the surfaces of composite and lithium metal electrodes may be expected to be quite variable.

System modeling[4] of lithium polymer[7] and lithium ion polymer batteries[5,6] shows that during the discharge and charge of these batteries, substantial concentration gradients develop within the composite electrodes and adjacent to the lithium electrode. Depletion effects are known to initiate dendrite growth[22] at lithium metal and to limit the usable capacity of the composite electrode[44]. The effect of high salt concentrations next to surfaces has mostly been considered in terms of salt precipitation[45] which represents a change in physical state. However, from the consideration of the behavior of t_g with salt concentration and inhibition of chain segmental motion next to surfaces outlined above, a simpler state change to the glassy form could also occur before precipitation. In either case an immobile and poorly conducting layer is formed next to the electrode that can involve a large proportion of the electrolyte in a composite electrode if the particle sizes are small enough. Once formed, these immobile layers will relax quite slowly leading to a build up with cycling of the resistive layer and this will

lead to losses in capacity utilization due to an increase in the cathode impedance. An example of this effect is given in Figure 5 which shows the capacity fading behavior of a Li/PEO-LiTFSI(8:1)/V_6O_{13} cell cycled at 0.1 mA/cm^2 at 85^{o}C (Figure 5a) and the development of the impedance spectrum during cycling (Figure 5b). In this particular case, the fading is exaggerated due to effects involved with obtaining the impedance spectra which appear to have caused some damage to the cell. That this fading is mostly due to electrolyte transport effects may be demonstrated by improvements in the capacity fade rate brought about by variation of the electrode thickness and by replacement of the electrolyte with other polymers containing different salt concentrations and which have improved transport and interfacial properties. Increased temperature was also observed to improve the fading problem which is also consistent with better transport properties. The case of the high capacity V_6O_{13} appears to be different from the lower capacity Li_xMnO_2 where depletion effects dominate[45,46] but both cases demonstrate the significant effect that poor electrolyte transport properties have upon capacity utilization and fading. Clearly phase changes that are induced by concentration gradients next to the electrodes will depend on the transport properties of the electrolyte, the current density used and the duration of the discharge or charge in addition to the material properties of the polymer (t_g). Changes in the composite electrode formulation (different loadings of carbon, active material, particle sizes, modification of the surfaces[47]) result in better performance and, indeed, the capacity retention of V_xO_y cathodes have been considerably improved by these means.

Although these interfacial effects appear to be intuitively reasonable for composite electrodes with very high surface areas, it is less obvious that they would

greatly affect planar electrodes such as lithium metal if the current density is kept well below the limiting current[48]. However, Figures 6, 7 and 8 demonstrate that even at a planar lithium electrode the interfacial effects can be considerable. Figure 6 shows the polarization behavior of a symmetrical lithium/$P(EO)_{30}$-LiTFSI/lithium cell at 85°C polarized six times at 0.2 mA/cm^2 for a charge of 2.75 coulombs/cm^2 in the same direction. In this case the PEO polymer has a M_w of 4 x 10^6 and contains 4% fumed silica and calcium salts (lab purified – see experimental). The polymer electrolyte membrane was very thick in this case (500 μm) with a low limiting current (ca. 0.25 mA/cm^2). After the polarization was terminated, the impedance spectrum of the cell was recorded beginning 30s after polarization was terminated. The cell was then allowed to relax for one hour following recording of the impedance spectrum when a second impedance spectrum was recorded. Polarization was then repeated. The impedance spectra recorded immediately after polarization and after the one hour relaxation are shown in Figure 7. One can see that size of the semi-circle measured 30s (a) after the current is terminated changes with cycling in a quite unpredictable fashion but tends to return to the same value after the one hour relaxation (Figure 7(b)). This indicates that little irreversible chemical reaction occurs during polarization and at least some portion of the interfacial impedance is due to salt concentration gradients at the electrodes that relax with time. This short-term behavior is not the same as SEI growth due to long-term corrosion[49] and is consistent with observation of little SEI growth during full cell cycling[45]. The continued increase in the polarization of the cell observed in Figure 6 indicates that even a one hour rest is insufficient to fully relax the concentration gradients in this cell, which is a very thick cell designed to exaggerate the effects of the transport properties.

Figure 8 demonstrates the difference that the cell geometry plays in the development of concentration gradients. Figure 8a shows the cycling of a symmetrical Li/P(EO)$_{30}$-LiTFSI/Li cell with a separator thickness of 38 μm and a steady-state limiting current of 2.5 mA/cm^2 while Figure 8b shows a cell with separator thickness of 265 μm and a limiting current of 0.36 mA/cm^2. The cells are cycled at 0.2 mA/cm^2 at 85^{o}C for 2 coulombs/cycle with a one hour rest between polarizations. In the case of the thin cell the polarization is only 25 mV during the first few cycles but this grows on cycling until at cycle 21 the voltage does not reach a steady value but rises quite steeply and the cell short circuits due to growth of a dendrite. With the thick cell, the polarization is considerably larger on cycle 1 (200mV), increases upon cycling and rapidly fails to reach a steady value. By cycle 16, there is a large polarization which appears to be close to transition time behavior. Some roughening change of the electrode surface then occurred that lead to a change in the electrode area or separator thickness. This reduced the polarization to allow the cell to continue cycling. The cell finally short-circuits in cycle 52. The thicker separator with better mechanical properties apparently prevented a short circuit due to dendrite growth for a considerable time but the electrode shape changes to reduce the polarization.

Another series of cells was built with higher salt concentrations (8:1) and cycled under the same conditions. Although these cells had steady state limiting currents nearly four times higher than the cells in Figure 8 they all rapidly grew dendrites on the first polarization cycle. The cell polarization dropped to low values indicative of changes in the electrode geometries although the cells did not completely short out. This is contrary to expectation if salt depletion drives the dendrite growth but could be consistent with a

concentration–dependent phase change at the anode. The growth of a less mobile layer next to the anode resulting from the cross-linking effects of the high salt concentration generated by the concentration gradient combined with the strong interactions between the polymer electrolyte and the constituents of the SEI layer on the lithium metal will result in a steady increase in the impedance of the cell. It is postulated that the growth of such a layer may not be uniform across the electrode surface thereby leading to variations in the secondary current distribution, a condition that favors the initiation of dendrite growth. The growth of a less mobile and more resistive layer at the counter electrode will reduce the limiting current of the cell below that expected form the bulk electrolyte transport properties and the cell geometry. Since it is also possible that the rate of growth of such a layer will not be uniform and may well reflect non-uniformities already present on the electrode, then it would not be unreasonable to expect non-uniformity to develop in the current distribution at the plating electrode. Although a decrease of the local limiting current below the operating current could occur, it is apparently not necessary to exceed the limiting current to initiate and propagate dendrite growth[28] and the changes that occur in polymer mobility due to concentration effects at surfaces may well be enough to reduce the critical current density to initiate dendrite growth.

Conclusion.

Polymer chain motion in polymer electrolytes is affected by the presence of surfaces. In dry polymer electrolytes this usually leads to decreases in lithium ion transport and poorer performance of the cell. The generation of salt concentration gradients due to binary salts with inadequate transport properties leads to increased concentrations of salt next to the electrodes and this compounds the effect of the surface

on the polymer motion. Both capacity and power capability are impacted by these effects. This implies that polyelectrolyte single-ion conductors will perform better since they do not generate concentration gradients. The question then is whether the polyelectrolytes remain mobile at the surface and do not self-assemble into a non-conducting layer on the electrode surface. The results shown here also imply that polymers based on ethylene oxide units are not optimum for interfacial behavior. Figure 4 shows that the polymer PTMO shows a much smaller dependence of t_g on salt concentration. This confirms some recently reported results on comb-branch polymers containing TMO groups[50]. The results described in this paper indicate that much improved behavior should be expected with TMO-containing polymers, and polyelectrolytes. The results of experiments on these materials will be reported in forthcoming publications.

Acknowledgement. This work was supported by the Assistant Secretary for Energy Efficiency and Renewable Energy, Office of FreedomCAR and Vehicle Technologies of the U.S. Department of Energy under Contract No. DE-AC03-76SF00098

References

1. G. Tsagaropoulos; A. Eisenberg. Macromolecules 28*(*1995), 6067.
2. A. Zhu; S. S. Sternstein. "Nanofiller-Polymer Interactions at and above the Glass Transition Temperature"; MRS, 2000, Boston, MA.
3. W. E. Wallace; J. H. Vanzanten; W. L. Wu. Physical Review A 52*(*1995), R3329.
4. K. E. Thomas; R. M. Darling; J. Newman. Mathematical Modeling of Lithium Batteries. In *Advances in lithium-ion batteries;* Schalkwijk, W. A. v.; Scrosati, B. Eds.; Kluwer Academic/Plenum Publishers: New York, NY, 2002; pp. 345.
5. M. Doyle; J. Newman; A. S. Gozdz; C. N. Schmutz; J. M. Tarascon. Journal of the Electrochemical Society 143*(*1996), 1890.
6. P. Arora; M. Doyle; A. S. Gozdz; R. E. White; J. Newman. Journal of Power Sources 88*(*2000), 219.
7. K. E. Thomas; S. E. Sloop; J. B. Kerr; J. Newman. Journal of Power Sources 89*(*2000), 132.
8. F. Croce; G. B. Appetecchi; L. Persi; B. Scrosati. Nature V394*(*1998), 456.
9. L. Persi; F. Croce; B. Scrosati; E. Plichta; M. A. Hendrickson. Journal of the Electrochemical Society V149*(*2002), A212.
10. H. J. Walls; J. Zhou; J. A. Yerian; P. S. Fedkiw; S. A. Khan; M. K. Stowe; G. L. Baker. Journal of Power Sources V89*(*2000), 156.
11. A. S. Best; A. Ferry; D. R. MacFarlane; M. Forsyth. Solid State Ionics 126*(*1999), 269.
12. A. S. Best; J. Adebahr; P. Jacobsson; D. R. MacFarlane; M. Forsyth. Macromolecules 34*(*2001), 4549.
13. J. Adebahr; A. S. Best; N. Byrne; P. Jacobsson; D. R. MacFarlane; M. Forsyth. Physical Chemistry Chemical Physics 5*(*2003), 720.
14. M. Forsyth; D. R. MacFarlane; A. Best; J. Adebahr; P. Jacobsson; A. J. Hill. Solid State Ionics 147*(*2002), 203.
15. B. Kumar; L. G. Scanlon; R. J. Spry. Journal of Power Sources 96*(*2001), 337.
16. B. Kumar; S. J. Rodrigues. Journal of the Electrochemical Society V148*(*2001), A1336.

17. B. Kumar; L. Scanlon; R. Marsh; R. Mason; R. Higgins; R. Baldwin. Electrochimica Acta V46*(*2001), 1515.
18. Y. Aihara; G. B. Appetecchi; B. Scrosati. Journal of the Electrochemical Society 149*(*2002), A849.
19. Y. Aihara; G. B. Appetecchi; B. Scrosati; K. Hayamizu. Physical Chemistry Chemical Physics 4*(*2002), 3443.
20. M. Rosso; T. Gobron; C. Brissot; J. N. Chazalviel; S. Lascaud. Journal of Power Sources 97-8*(*2001), 804.
21. C. Brissot; M. Rosso; J. N. Chazalviel; S. Lascaud. Journal of Power Sources 94*(*2001), 212.
22. O. Buriez; Y. B. Han; J. Hou; J. B. Kerr; J. Qiao; S. E. Sloop; M. M. Tian; S. G. Wang. Journal of Power Sources 89*(*2000), 149.
23. J. L. Barton; J. O. M. Bockris. Proc R.Soc. London, Ser. A 268*(*1962), 485.
24. M. Dolle; L. Sannier; B. Beaudoin; M. Trentin; J. M. Tarascon. Electrochemical & Solid-State Letters 5*(*2002), A286.
25. L. G. Sundstrom; F. H. Bark. Electrochimica Acta 40*(*1995), 599.
26. J.-i. Yamaki; S.-i. Tobishima; K. Hayashi; K. Saito; Y. Nemoto; M. Arakawa. J. Power Sources 74*(*1998), 219.
27. J. O. Besenhard; J. Guertler; P. Komenda; M. Josowicz. Proc. - Electrochem. Soc. 88-6*(*1988), 618.
28. C. Monroe; J. Newman. Journal of the Electrochemical Society 150*(*2003), A1377.
29. T. Tatsuma; M. Taguchi; N. Oyama. Electrochimica Acta 46*(*2001), 1201.
30. E. Peled. Journal oof the Electrochemical Society 126*(*1979), 2047.
31. J. Xie; R. Duan; J. B. Kerr. Journal of the Electrochemical Society Submitted*(*2003).
32. G. Tsagaropoulos; A. Eisenberg. Macromolecules 28*(*1995), 396.
33. S. Gagliardi; V. Arrighi; R. Ferguson; M. T. F. Telling. Physica B 301*(*2001), 110.
34. E. A. Turi. Thermal Characterization of Polymeric Materials,; Academic Press.: San Diego, CA, 1997; Vol. 1.

35. J. D. Ferry *Viscoelastic Properties of Polymers*, 3rd ed.; Wiley: New York, NY, 1980.
36. J. M. G. Cowie *Polymer: Chemistry and Physics of Modern Materials*, 2nd. ed.; Blackie: London, 1991.
37. J. E. Weston; B. C. H. Steele. Solid State Ionics 7*(*1982).
38. M. A. Ratner. Polymer electrolyte reviews--1*;* MacCallum, J. R.; Vincent, C. A. Eds.; Elsevier Applied Science: London ; New York, 1987; pp. x.
39. M. A. Ratner; P. Johansson; D. F. Shriver. Mrs Bulletin 25*(*2000), 31.
40. J. E. Weston; B. C. H. Steele. Solid State Ionics 7*(*1982), 81.
41. M. M. Doeff; L. Edman; S. E. Sloop; J. Kerr; L. C. De Jonghe. Journal of Power Sources 89*(*2000), 227.
42. L. Edman; M. M. Doeff; A. Ferry; J. Kerr; L. C. De Jonghe. Journal of Physical Chemistry B 104*(*2000), 3476.
43. J. B. Kerr; S. E. Sloop; G. Liu; Y. B. Han; J. Hou; S. Wang. Journal of Power Sources 110*(*2002), 389.
44. M. Doyle; T. F. Fuller; J. Newman. Electrochimica Acta 39*(*1994), 2073.
45. L. Edman; M. M. Doeff. Solid State Ionics 158*(*2003), 177.
46. M. M. Doeff; A. Ferry; Y. P. Ma; L. Ding; L. C. Dejonghe. Journal of the Electrochemical Society 144*(*1997), L 20.
47. L. F. Nazar; G. Goward; F. Leroux; M. Duncan; H. Huang; T. Kerr; J. Gaubicher. International Journal of Inorganic Materials 3*(*2001), 191.
48. J. Newman *Electrochemical Systems*; Prentice-Hall: Englewood Cliffs, NJ, 1991.
49. B. Laik; L. Legrand; A. Chausse; R. Messina. Electrochimica Acta 44*(*1998), 773.
50. J. B. Kerr; G. Liu; L. A. Curtiss; P. C. Redfern. Electrochimica Acta 48*(*2003), 2305.

List of Figures.

Figure 1. Schematic representations of inhibition of polymer segmental motion by filler particle surfaces. a) black shading represents immobilized polymer on the filler particle surface, grey shading represents restricted mobility polymer layers[1]. b) long polymer chains interact with more than one particle leading to reduced mobility through out the polymer[2].

Figure 2. Dynamic Mechanical Thermal Analysis of PPO with added fumed silica (A200). Tan δ against temperature, recorded at 10hz and at 10^{o}C/min. The legend denotes the % by weight of fumed silica added to the polymer.

Figure 3. Schematic representation of a Lithium metal-polymer electrolyte-composite electrode showing active intercalation compound particles (ca. 1-10 μm) and carbon black particles (20-40nm).

Figure 4. Dependence of glass transition temperature (t_g) of PEMO, PPO and PTMO on salt concentration (shown at the ratio of oxygen concentration to lithium ion concentration). Neat polymer with no salt added is plotted as 100:1 for convenience.

Figure 5. (a) Cycling capacity of Li/P$(EO)_{30}$-LiTFSI/V_6O_{13} with cycle number. Discharged and charged at 0.1mA/cm^2at 85^{o}C. Weight of active material in cathode =

30% by weight (1.26mg), 10% weight carbon black, 2% Brij, 58% $P(EO)_{30}$-LiTFSI. (b) Impedance spectra taken during cycling of the cell shown in (a). PEO is lab purified.

Figure 6. Polarization behavior of a $Li/P(EO)_{30}$-LiTFSI/Li cell at 85°C. Six successive polarizations in same direction at 0.2 mA/cm^2 for 2 coulombs each. Impedance spectra (see Figure 7) and one hour polarization between polarizations. PEO is lab purified

Figure 7. Impedance spectra recorded on cell shown in Figure 6 from 65khz to 0.1hz after polarizations. (a) recorded 30 seconds after polarization terminated. (b) recorded one hour after the impedance spectra in (a).

Figure 8. Polarization behavior of $Li/P(EO)_{30}/Li$ cells cycled symmetrically at 0.2 mA/cm^2 at 85°C for 2 coulombs /cycle. One hour rest between polarizations. Cell thickness (a) 38µm. (b) 265µm.

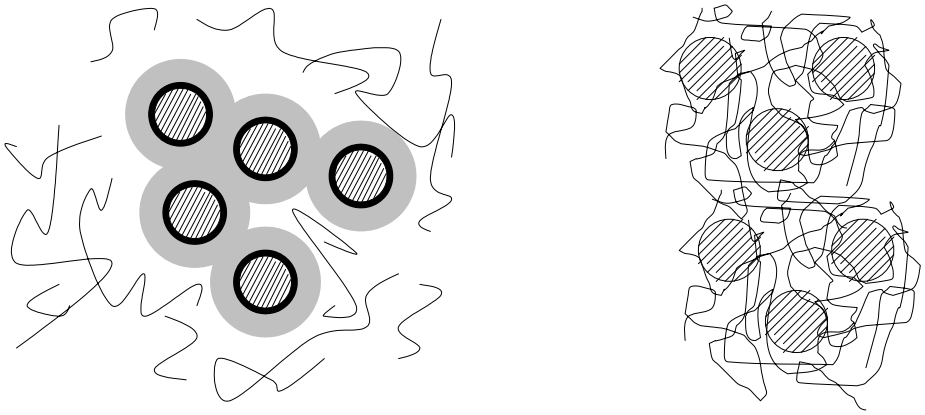

(a) **(b)**

Figure 1

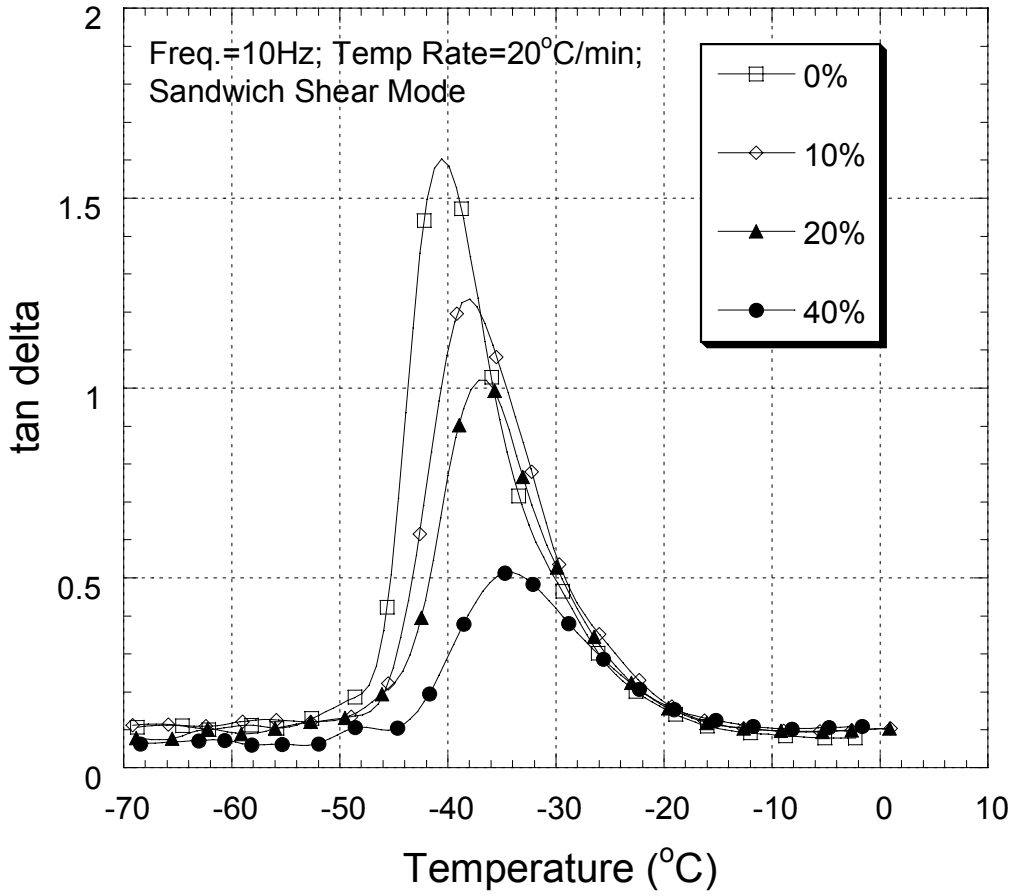
Freq.=10Hz; Temp Rate=20°C/min;
Sandwich Shear Mode
0%
10%
20%
40%
tan delta
Temperature (°C)
2
1.5
1
0.5
0
-70
-60
-50
-40
-30
-20
-10
0
10

Figure 2

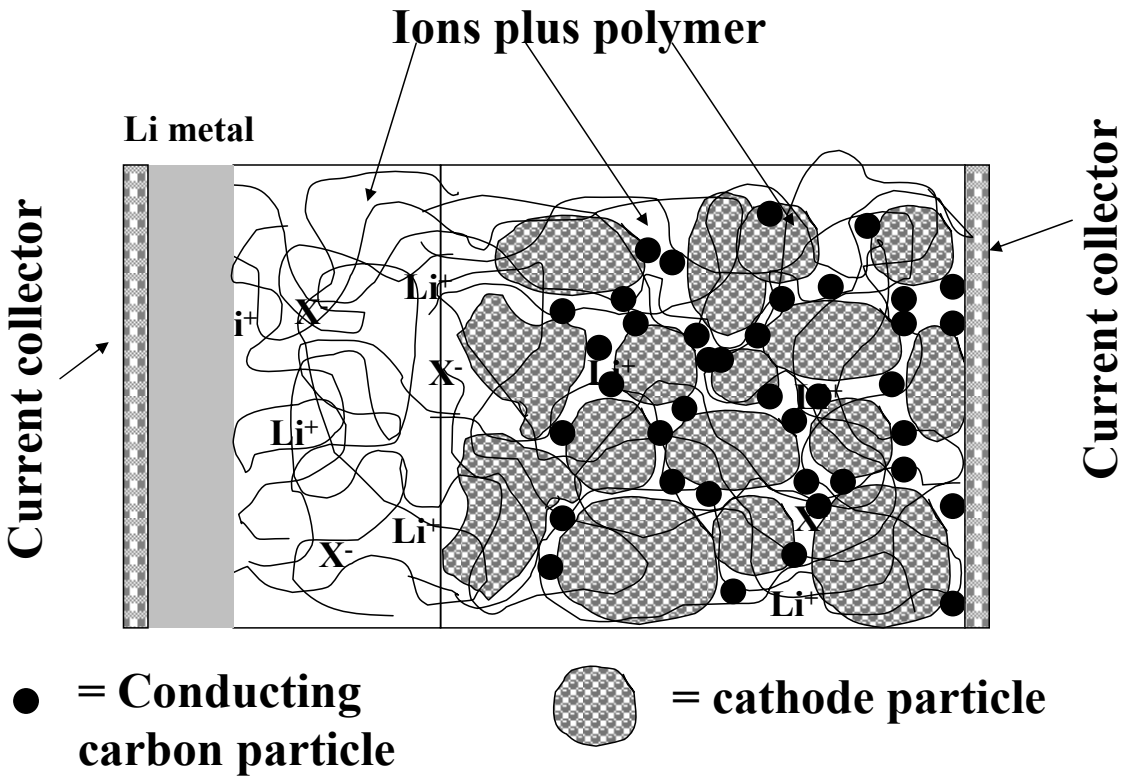
Ions plus polymer
Li metal
Current collector
Current collector
Li+
X-
Li+
X-
Li+
Li+
X-
Li+
= Conducting carbon particle
= cathode particle

Figure 3

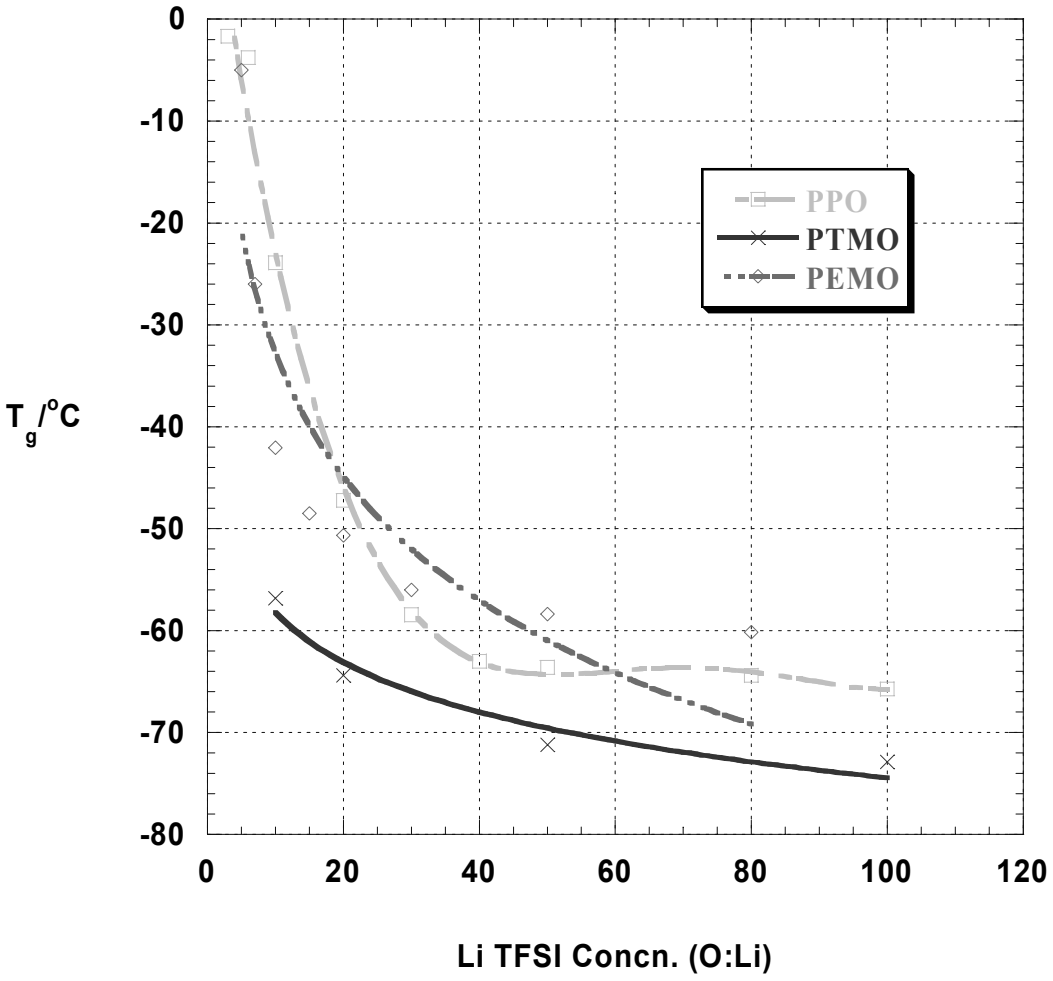
0
-10
-20
-30
-40
-50
-60
-70
-80
0
20
40
60
80
100
120
T g /°C
Li TFSI Concn. (O:Li)
PPO
PTMO
PEMO

Figure 4.

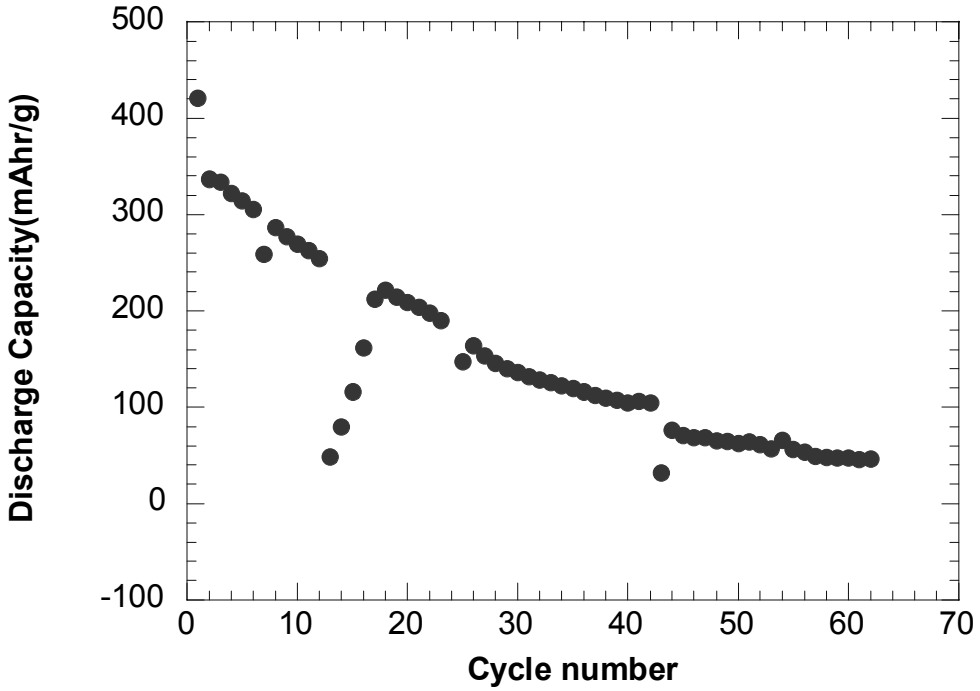
Discharge Capacity(mAhr/g)
Cycle number
500
400
300
200
100
0
-100
0
10
20
30
40
50
60
70

(a)

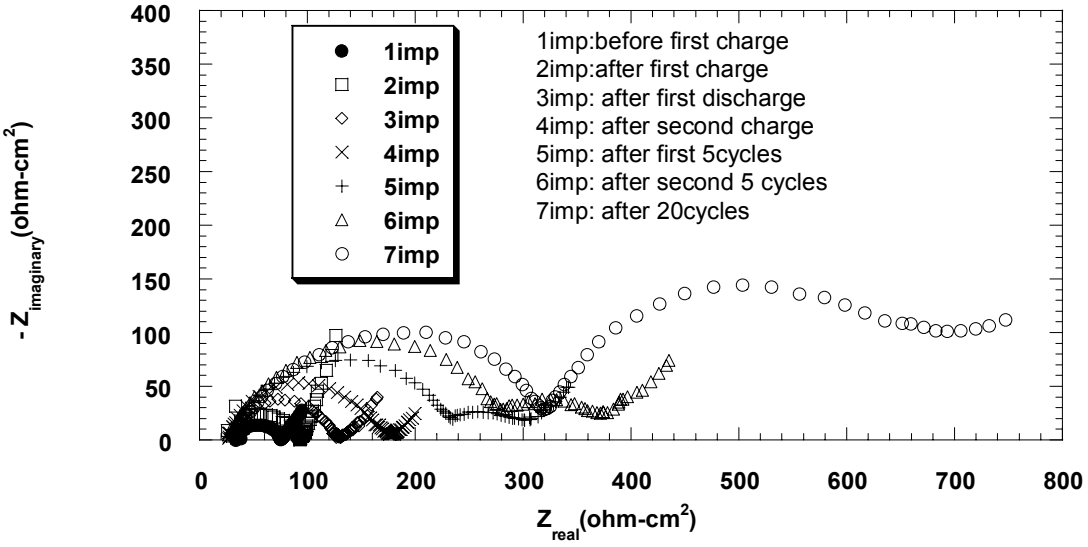
1imp
2imp
3imp
4imp
5imp
6imp
7imp
1imp:before first charge
2imp:after first charge
3imp: after first discharge
4imp: after second charge
5imp: after first 5cycles
6imp: after second 5 cycles
7imp: after 20cycles
- Z imaginary (ohm-cm2)
Z real (ohm-cm2)
400
350
300
250
200
150
100
50
0
0
100
200
300
400
500
600
700
800

(b)

Figure 5

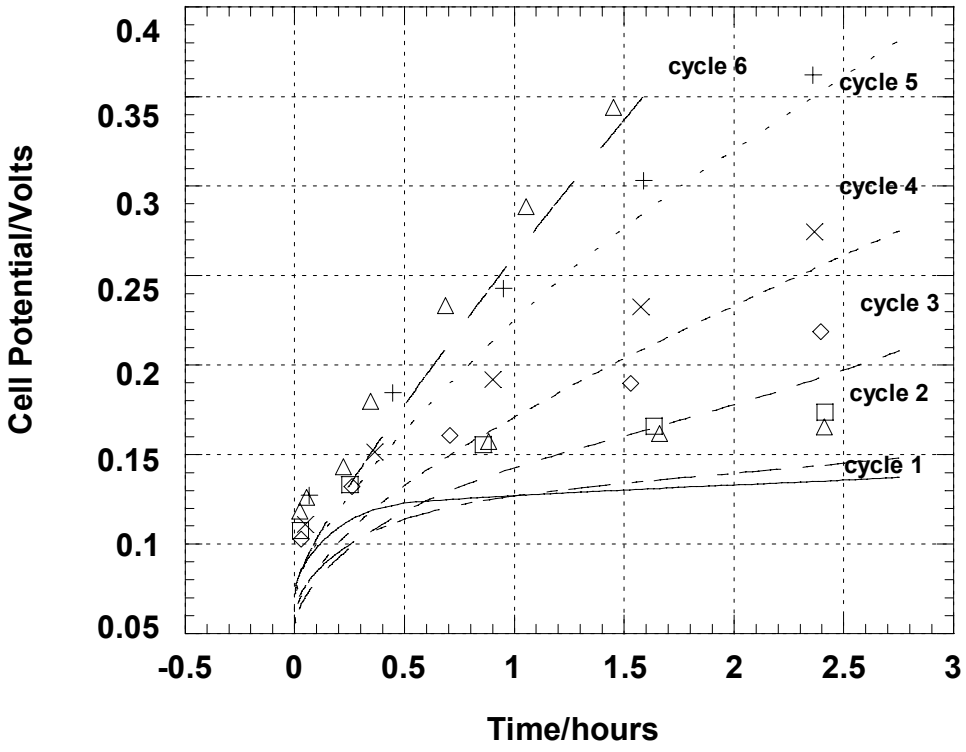
Cell Potential/Volts
Time/hours
0.4
0.35
0.3
0.25
0.2
0.15
0.1
0.05
-0.5
0
0.5
1
1.5
2
2.5
3
cycle 6
cycle 5
cycle 4
cycle 3
cycle 2
cycle 1

Figure 6

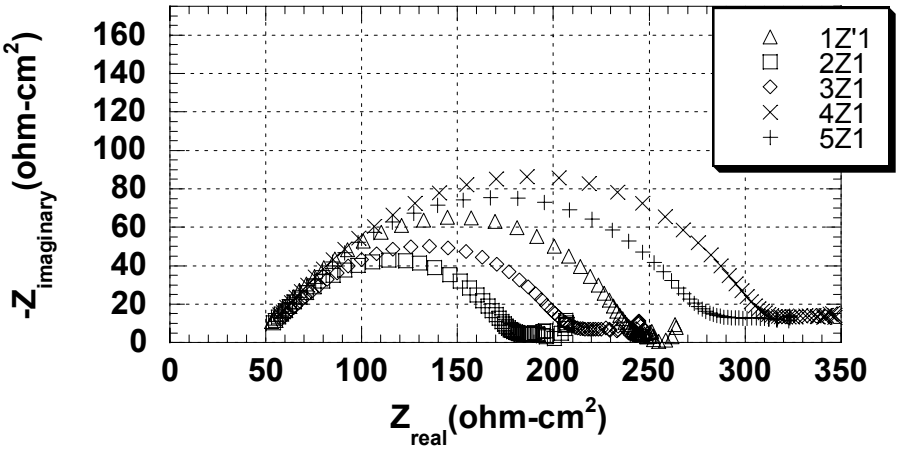
-Z imaginary (ohm-cm2)
Z real (ohm-cm2)
1Z'1
2Z1
3Z1
4Z1
5Z1

(a)

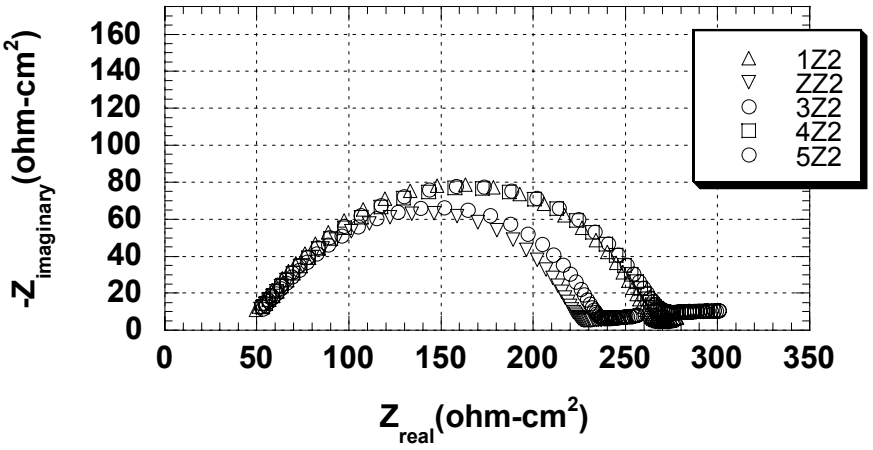
-Z imaginary (ohm-cm2)
Z real (ohm-cm2)
1Z2
ZZ2
3Z2
4Z2
5Z2

(b)

Figure 7

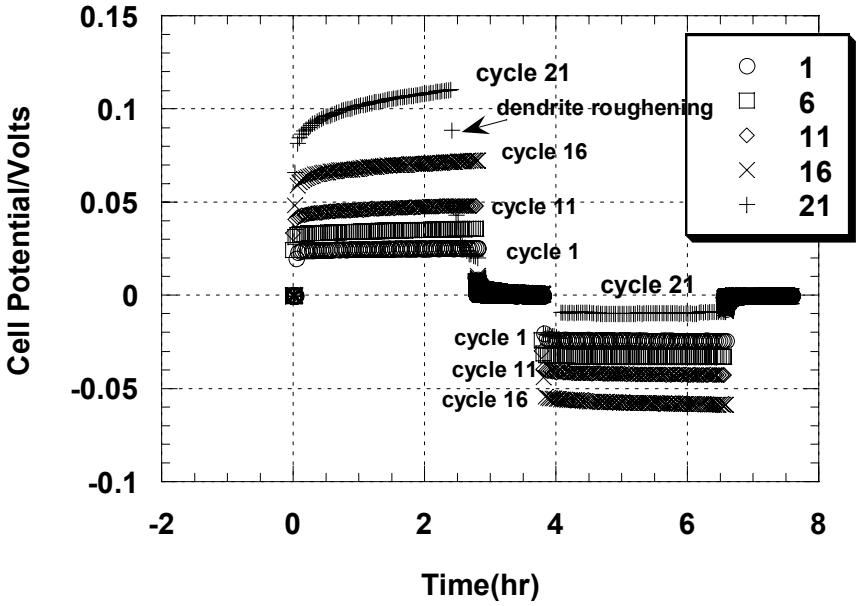
0.15
0.1
0.05
0
-0.05
-0.1
-2
0
2
4
6
8
Cell Potential/Volts
Time(hr)
cycle 21
dendrite roughening
cycle 16
cycle 11
cycle 1
cycle 21
cycle 1
cycle 11
cycle 16
1
6
11
16
21

(a)

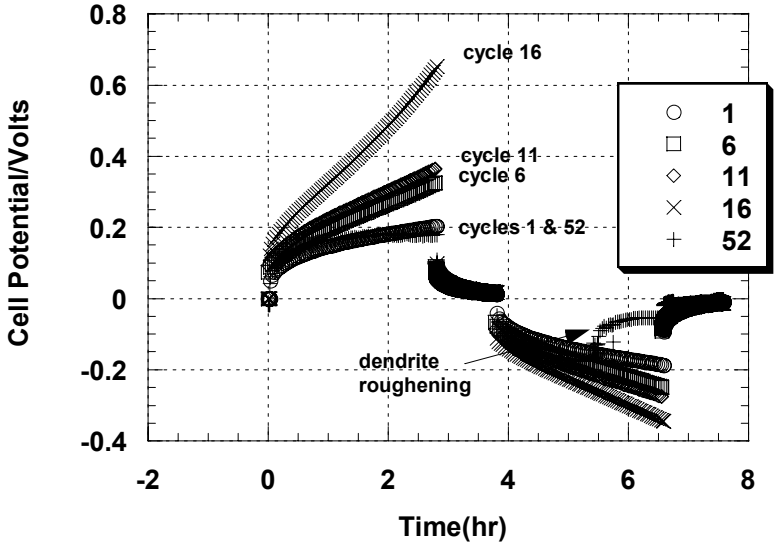
0.8
0.6
0.4
0.2
0
-0.2
-0.4
-2
0
2
4
6
8
Cell Potential/Volts
Time(hr)
cycle 16
cycle 11
cycle 6
cycles 1 & 52
dendrite
roughening
1
6
11
16
52

(b)

Figure 8